Insights in Emerging $Ti_3C_2T_x$ MXene-Enriched Polymeric Coatings for Metallic Surface Protection: Advancements in Microstructure, Anti-Aging, and Electrochemical Performance

Xingyu Wang [a], Sampada Koirala [b], Luyang Xu [a], Qiaobin Li [d], Zhibin Lin [a], Xiaoning Qi [c], Ying Huang [a], Zhongyu Yang [d], and Danling Wang [b]*

[a] *Department of Civil, Construction, and Environmental Engineering, North Dakota State University, Fargo, ND 58108, USA*

[b] *Department of Electrical and Computer Engineering, North Dakota State University, Fargo 58108, ND, USA*

[c] *Department of Coatings and Polymeric Materials, North Dakota State University, Fargo, ND 58018, USA*

[d] *Department of Chemistry and Biochemistry, North Dakota State University, Fargo, ND 58108, USA*

** Corresponding author: North Dakota State University, 1340 Administration Ave., Fargo, ND 58108, USA, Email: danling.wang@ndsu.edu; Phone:701-231-8396; ORCID number: 0000-0003-0119-441X.*

Abstract

This study provides new insights into the development of high-performance MXene-reinforced coatings to strengthen polymeric nanocomposites by enhancing microstructure, anti-aging properties, corrosion resistance, and robustness. MXene nanoparticles, labeled 25C and 80C, were synthesized using two different methods and incorporated at concentrations ranging from 0.1 to 2.0 wt.% into epoxy composites. The results demonstrated that 80C MXene, characterized by its finer morphology and superior dispersion, significantly improved the composite's performance compared to 25C. Electrochemical Impedance Spectroscopy (EIS) tests, along with long-term exposure assessments, suggested that incorporating both types of MXene nanoparticles enhances the corrosion protection performance of epoxy coatings over time. Micro-CT analysis revealed that both types of MXene substantially reduced defects and voids in the polymeric matrix, resulting in enhanced protective performance. This void reduction confirms that the incorporation of both 25C and 80C MXene improves microstructural integrity by filling voids and creating a more continuous, uniform structure, particularly in samples with 0.1% to 1.0% MXene flakes. The findings also highlighted MXene's potential in modifying the anti-aging properties of epoxy by inhibiting free radical generation and enhancing the composite's resistance against corrosion. Both 25C and 80C MXene-epoxy groups exhibited a clear trend of diminishing free radical intensity with increasing MXene concentration up to 1.0%, with free radical intensity reduced by over 40% compared to neat epoxy. The relationship between MXene concentration and reinforcement was also investigated, revealing superior corrosion protection properties at concentrations of 0.5-1.0 wt.%. This research offers a profound understanding of MXene's potential in polymer-based composites, laying a foundation for future investigations aimed at utilizing MXene to achieve superior material properties for a wide range of applications, particularly in the realm of metallic surface protection.

Keywords: MXene, High-performance, Polymer-matrix composites (PMCs), Microstructures, Anti-aging,

1. Introduction

Despite significant efforts in advancing polymeric coatings, particularly for corrosion protection and durability, premature coating failures are frequently encountered, leading to early-stage structural damage

induced by corrosive attacks. MXene, a 2D graphene-like nanomaterial, exhibits exceptional physical and chemical properties that have garnered significant attention from researchers and industries in recent years [1–4]. With the exceptional 2D flake structure and chemical functionality, MXene and MXene-based materials can be integrated into polymeric composites to fabricate high-performance materials that meet the requirements of cutting-edge applications [5].

MXene-based nanomaterials are transition metal carbides and/or nitrides, which were discovered by Naguib et al., in 2011 from Ti_3AlC_2 MAX phase, and have attracted more attention as a new material in the recent decade [6,7]. MXenes were exfoliated from MAX phases, which not only inherited properties from parent materials, but also simultaneously demonstrated other intriguing properties [1,8]. The MAX phase, which combines metal and nonmetal elements under high-temperature conditions, shows high thermal and mechanical stability, as well as electrical conductivity from the metallic bonding [1]. On the other hand, MXenes are layered materials that have a metallic or semi-conducting behavior, and are known for their excellent electrical conductivity, mechanical strength, and chemical stability. If used as nanofillers, MXene nanoparticles offer several advantages over traditional nanoparticles in reinforcing polymeric coatings. Firstly, the 2D structure and high aspect ratio of MXene can contribute to the formation of a robust network within the polymer matrix, resulting in enhanced mechanical properties and barrier performance [9,10]. Secondly, the presence of diverse surface functional groups on MXene enables stronger interfacial interactions between the nanofiller and the polymer, which has the potential to improve the overall performance of the composite coatings [11].

Owing to their distinctive properties and wide-ranging potential applications, MXene-based polymeric composites have drawn significant research attention in recent years, and many scientists are working to explore their potential and develop new technologies based on these materials. MXenes are arguably the fastest growing 2D materials in the post-graphene era. Since their discovery in 2011 [12,13], they have attracted widespread research interest due to their intriguing electrical, thermal, mechanical, and chemical properties [14]. Based on the data retrieved from the Web of Science, the terms "MXene nanocomposite" and "MXene coating" in scientific publications have seen a remarkable increased in recent years, showcasing an exponential growth of the field, as evidenced by the yearly increase in the number of related papers published (Fig. 1).

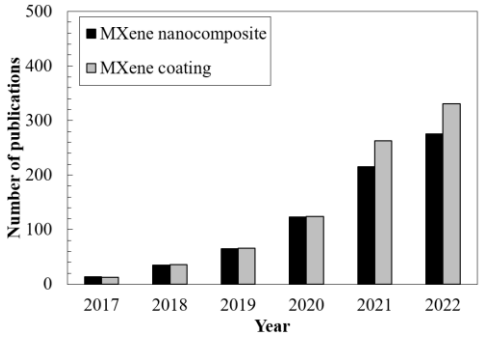

Figure 1. The scientific publications with the keywords of "MXene nanocomposite" and "MXene coating", results were obtained from the Web of Science.

The findings in researchers' previous investigations agreed that, 2D MXenes became an ideal nanofiller for fabricating high-performance polymer composites that can meet the electrical, thermal, mechanical, flame-retardant and other intriguing properties [15,16]. On the other hand, one thing that should be noticed is that MXenes have trouble in the application process by itself, as they are easy to be oxidized in the air, such as the formation of TiO_2; another challenge is that the MXenes are easy to restack. Both of the challenges can be overcome when using MXene as a nanofiller and directly dispersed into polymeric resin, as 1) the oxidization of MXene will be inhibited as they are covered by polymeric matrix, and 2) the high viscosity of polymeric resin will mitigate dispersed MXene from restacking. Therefore, the application of MXene into polymeric coating shows great potential. Researchers agreed that, among the numerous MXene materials, $Ti_3C_2T_x$ is the most widely used due to its excellent chemical and mechanical properties [17,18]. Compared with other traditional two-dimensional materials, the active surface groups of $Ti_3C_2T_x$, such as F, O, OH, and Cl, make it possible to well interacting with the organic polymers through covalent bonds, electrostatic interactions, van der Waals forces or hydrogen bonds [19]. Therefore, MXene-based nanocomposite, as new-generation coatings, are designed to provide high-performance, and multi-functional protective films that have excellent properties in corrosion-resistance, mechanical properties, antimicrobial, durability, and etc.

Along the research going with MXene, the application of MXene in areas such as water filtration, electromagnetic shielding, sensors, energy storage and catalyst, etc have been attracted ever-increasing attention and has also been extensively studied [20–24]. For example, Chen et al. summarized the current situation of MXene/polymer nanocomposites and reviewed the applications of MXene/polymer composites in energy, sensing, electromagnetic shielding and biomedical fields [25]. However, the research on MXene-based polymer composites is still in the early stages, and diverse performances need to be explored further [1]. Keep

exploring the development of MXene nanocomposite will undoubtedly discover and unlock the full potential of MXene-based composite coatings.

In recent years, several studies have been performed to investigate the utilization of MXene or MXene-based composites as coatings to provide protection to infrastructures. Qiang et al. investigated the inclusion of graphene oxide (GO)/Ti3C_2T_x nanosheets into epoxy coatings, and the results indicated that GO-$Ti_3C_2T_x$ nanosheets acted as effective nanofillers, providing a stronger physical barrier against corrosion for steel in 3.5 wt.% NaCl solution at different pressures. The impedance value for GO-$Ti_3C_2T_x$/EP remained at 1.84×10^8 Ω cm² after 8 days of immersion at 5 MPa, which was two orders of magnitude higher than that of pure epoxy (EP). This study highlighted the enhanced anti-corrosion performance of GO-functionalized MXene coatings; however, a reduction in corrosion resistance was observed after 8 days of exposure [26]. Cao et al. developed a $Ti_3C_2T_x$/silane composite coating using a solution-based process and examined its corrosion resistance performance and mechanism. The $Ti_3C_2T_x$ nanosheets effectively minimized micro-voids and extended the diffusion pathway for corrosive media. After 30 days of immersion in a 3.5 wt% NaCl solution, the $Ti_3C_2T_x$/silane composite coating maintained excellent anti-corrosion performance with a high protection efficiency of 98.55%. This study demonstrated the remarkable improvement in corrosion resistance provided by $Ti_3C_2T_x$ MXene in silane composite coatings on copper [27]. Moreover, Lou et al. also employed electrochemical methods to evaluate the anticorrosion properties of nanocomposite coatings on copper substrates. Their findings revealed that the polyurethane sample containing $Ti_3C_2T_x$ MXene and functionalized carbon nanotubes exhibited a significant reduction in corrosion rate. This study underscores the improved anti-corrosion properties of polyurethane nanocomposites through the incorporation of $Ti_3C_2T_x$ MXene and functionalized carbon nanotubes [28].

While previous studies have extensively explored the integration of various nanomaterials into epoxy matrices, there remains a notable gap in research that not only expands on the conventional understanding of polymer reinforcement but also introduces new dimensions related to microstructural stability and anti-aging properties under accelerated aging conditions. Furthermore, there appears to be a lack of comprehensive evaluation of nanofillers, particularly concerning particle size, dispersion, and their impact on the viscosity and microstructure of the composite. Additionally, most existing research has predominantly focused on a single MXene nanoparticle fabrication method. In contrast, our study delves into comparing two distinct MXene

synthesis methods and examines their impact on the performance of the resultant nanocomposites. By addressing these gaps, our research offers a nuanced understanding of how different synthesis conditions affect the dispersion quality, structural integrity, and functional performance of MXene within an epoxy matrix, thus providing significant insights into advanced materials engineering.

In this manuscript, the presented research aims to provide novel insights into the fabrication of high-performance MXene-reinforced coatings, in order to enhance the corrosion and durability of metal substrates. The MXene-reinforced epoxy coatings were evaluated by a comprehensive experimental study, which incorporated MXene nanoflakes into a solvent-free nanocomposite coating for corrosion protection on metallic surfaces. Two methods were used to fabricate MXene nanoparticles, and the products were labeled as 25C and 80C; additionally, both of them were employed as nano-fillers to fabricate epoxy-based nanocomposites. In order to find out the influence of MXene nanofiller concentration on the performance of the coating, nanocomposites were fabricated with varied concentrations of MXene (0.1, 0.5, 1.0, and 2.0 wt.%). Both types of MXene nanoparticles were homogeneously dispersed in the epoxy matrix, and the protective capabilities of developed MXene-epoxy composite coatings were investigated. This study employed micro-computed tomography (Micro-CT) to investigate the internal structure of MXene-epoxy nanocomposite, particularly evaluating void reduction by MXene. The corrosion resistance of MXene-based coatings was assessed using the Electrochemical Impedance Spectroscopy (EIS) test, and the durability was determined by employing the ASTM B117 salt spray accelerated weathering test. Additionally, Electron Spin Resonance (ESR) was utilized to track the production of free radicals and assess the anti-aging capabilities of the MXene-reinforced epoxy.

The obtained findings from this study, focusing on the development and analysis of MXene-enriched nanocomposites, marks a significant advancement in the field of materials science, particularly in the domain of polymer composites. The necessity of this work stems from the urgent need for materials that exhibit enhanced durability, structural integrity, and aging resistance under various environmental conditions. By integrating MXene into epoxy composites, the study not only addresses the prevalent issue of rapid degradation in traditional polymeric materials but also introduces a novel approach to enhancing protection properties. The investigation into the microstructural enhancements, anti-aging capabilities, and superior electrochemical behavior of MXene-epoxy composites underlines the potential of these materials to industries such as aerospace, automotive, and civil engineering. The groundbreaking insights provided by this research could lead to the

development of more resilient materials capable of withstanding harsh environmental challenges, thereby extending their lifespan and reducing maintenance costs.

2. Materials and experimental design

2.1. Synthesis of $Ti_3C_2T_x$ MXene

Preparation of MAX powder:

The MAX phases Ti_3AlC_2 particles were synthesized by ball milling TiC, Ti, and Al powders for 2 hours. The resulting powders were then pressed into a pellet and sintered at 1350 °C for 4 hours under argon flow. The collected pellets were then milled back into powder and sieved through a 160-mesh sieve. The MAX powder was then collected and stored in a small glass tube.

Preparation of MXene nanoparticles:

1) For 25C MXene: The minimally intensive layer delamination (MILD) method was used at a room temperature without any application of heat. Fluoride-based salt etchants were used to prepare in-situ HF. The etchant was prepared by adding 1.6 g of LiF to 15 mL of HCl and 5 mL of DI water, and then left under continuous stirring for 5 min. A total of 1.0 g of Ti_3AlC_2 powder was gradually added to the etchant above, and the reaction was allowed to run for 48 hours at room temperature of 25ºC.

2) For 80C MXene: Hydrothermal approach was used to prepare 80C MXene nanoparticles. Initially, the etchants were weighed out for LiF, HCl, and MAX using the same stoichiometric ratio for in-situ HF and were stirred on a stir plate using a Teflon bottle at room temperature for 1 hour. After that, the mixed solution was transferred into an autoclave and then placed in a tube furnace to a final heat up at 80ºC for 48 hours.

3) Final washing step for both 25C and 80C: Once the etching steps were completed after 48 hours, the washing steps were performed. During the washing process, the acidic mixtures were washed with DI water via centrifugation (5 min per 6000 rpm) for multiple cycles. The washing process continued until a pH of 4-5 was achieved.

2.2. Fabrication of MXene-epoxy nanocomposites

In this study, EPON 828 resin (Hexion Inc., USA), a bisphenol resin, was used as a liquid epoxy resin to fabricate the polymer to incorporate with MXene nanoparticles. EPIKURE Curing Agent 3175 (Hexion Inc., USA) was applied as the cross-linking agent to harden the epoxy resin. The process of fabricating

nanocomposites can be seen in Fig. 2. The MXene particles were dispersed into the epoxy resin using a combination of a high-shear disk mixer and ultrasonic dispersion. The MXene epoxy resin slurry was subjected to high-shear mixing at a controlled speed of 4000 rpm for 30 minutes. Subsequently, the mixture was sonicated with a Misonix S1805 ultrasonic system, following a 15-second "on/off" cycle at 100% amplitude for an overall duration of 30 minutes. To prevent overheating during the dispersion process, a water bath was employed. It is important to highlight that the MXene nanoparticles were dispersed into the epoxy resin immediately after fabrication. This method effectively mitigates the oxidation of MXene by ensuring that the nanoparticles are completely enveloped by the epoxy resin following the dispersion process. This encapsulation isolates the MXene from air exposure, significantly minimizing oxidation and preserving the integrity of the nanoparticles.

The curing agent was added to the mixture after dispersion, with a 1:1 mole ratio to the epoxy resin, and the mixing was carried out mechanically for 10 minutes at a speed of 600 rpm. The experimental investigation in the study involved the MXene-epoxy nanocomposites containing different weight contents of MXene, specifically 0.1, 0.5, 1.0, and 2.0 wt.% for both 25C and 80C MXenes. All the sample groups are denoted by the type and quantity of nanoparticles; for instance, 0.1%25C-E and 0.1%80C-E denote composites reinforced with 0.1% by weight of 25C and 80C MXene, respectively. Furthermore, a pure epoxy sample was utilized as a reference.

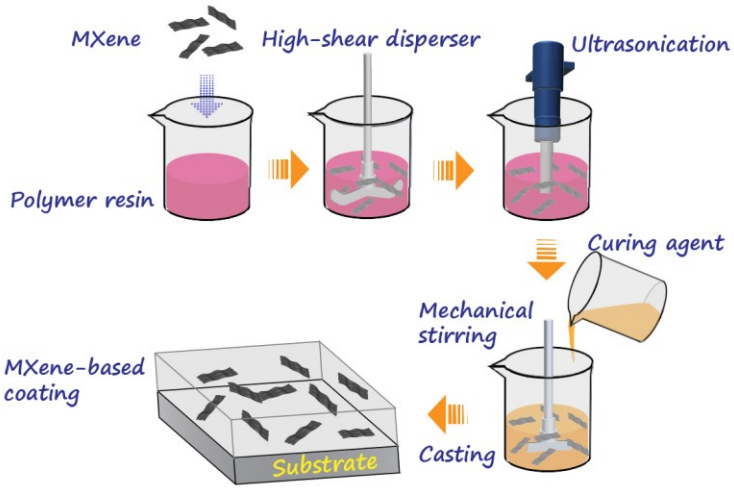

Figure 2. Schematic of the fabrication process of MXene-polymer nanocomposite.

2.3. Characterization of MXene nanoparticle and MXene-epoxy composite

Powder X-Ray Diffraction (XRD) patterns were captured by a Bruker AXS' D8 Discover multifunctional X-Ray Diffractometer, and the results were utilized to examine the structure of the MXenes. The particle size distribution MXenes was examined using the dynamic light scattering (DLS) method, which was carried out using a Nicomp 380 submicron particle sizer. The micrographs that were used in this study were produced with a field emission scanning electron microscope (FE-SEM), which a JSM-7600F Schottky was used. In addition, high-resolution analytical TEM equipment, JEM-2100, was employed to analyze the morphology and structures of the MXene nanoparticles.

2.4. Microstructure of nanocomposites using Micro-CT

Micro-CT, or micro-computed tomography, is a nondestructive imaging technology used to examine and analyze the internal structure of composite materials with a high degree of resolution. A micro-CT scan was used to assess the defect/voids in the MXene nanocomposite and to examine the interactions between MXene nanofiller and polymeric resin as well as the mechanisms of nanoparticle reinforcement. The investigation was conducted based on the void content and size of the voids; and the acquired data were then discussed together with the coating performance.

2.5. Electrochemical impedance spectroscopy test

The protection properties of the developed MXene nanocomposite coatings were investigated by Electrochemical impedance spectroscopy (EIS) test. The barrier properties of coating film and degradation of coated system were assessed by interpreting the EIS data via Bode and Nyquist plots. The EIS measurement was performed by a three-electrode cell, where the steel substrate (Q-panel) acts as the working electrode; and a platinum mesh and a saturated calomel electrode were employed as the counter electrode and reference electrode, correspondingly.

2.6. Accelerated durability test

Salt spray tests were used as an accelerated durability test to assess the developed coatings' corrosion resistance performance over a longer period of time. The ASTM B117 salt spray test is a widely accepted technique for assessing the corrosion resistance of materials or coatings, by subjecting the material or coating to a NaCl salt spray solution. This evaluation allows for the determination of a material's or coating's ability to

withstand corrosive environments. Consequently, the coating's long-term durability in a corrosive environment was assessed based on the EIS and Electron spin resonance (ESR) data gathered after varying hours of exposure.

2.7. Electron spin resonance (ESR) test

The capacity of MXene to delay the epoxy's aging progression was investigated using Electron Spin Resonance (ESR) analysis, performed on both neat epoxy and MXene-epoxy nanocomposites post exposure to salt spray. The ESR spectra were collected at ambient conditions using an ESR spectrometer, and this analysis was essential for identifying the formation of unpaired electrons, which were generated during the aging process.

3. Result and discussion

3.1. XRD patterns and morphologies of fabricated MXene

The XRD (X-ray diffraction) data presented in Fig. 3(a) shows two distinct patterns for MXene synthesized at 25C (red line) and 80C (black line). The produced 80C MXene exhibits a prominent (002) peak at 7.087°, indicative of a high-purity MXene phase, with additional peaks at 14.311° and 28.851° corresponding to (004) and Li_3AlF_6 phases, respectively. This suggests a successful etching process, corroborated by the minimal presence of Al and TiC impurities, leading to a conclusion that the etching of the MAX phase is more complete at this higher temperature. The presence of -OH groups as the surface-terminating groups further confirms the cleanliness of the MXene surface region [29].

In contrast, the 25C MXene displays a much weaker (002) peak, with discernible peaks at 35.985° and 44.96° suggesting the presence of TiC impurities, and peaks at 38.715° and 41.835° indicative of Ti_3AlC_2, a constituent of the original MAX phase [29,30]. This implies incomplete etching at the lower temperature, resulting in a less pure MXene with residual MAX layer components. The 80°C sample, in agreement with SEM results, shows the highest quality MXene, with peaks that confirm the formation of Li_3AlF_6 during the experiment, likely contributing to the debris observed in SEM image (Fig. 3 (b)).

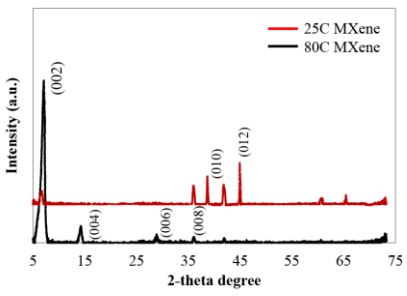

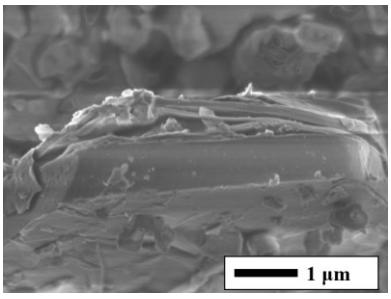

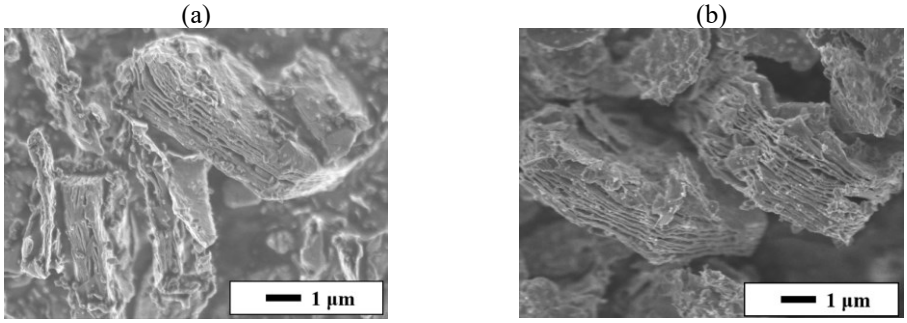

Figure 3. (a) XRD results of pure MXene samples, (b) MAX residuals found in 25C MXene, (c) exfoliated MXene sheets in 25C sample, and (d) exfoliated MXene sheets in 80C sample.

The SEM images in Fig. 3(c) and (d) displayed the exfoliated MXene sheets found in 25C and 80C MXene specimens. As demonstrated in the images, the etching procedure resulted in the removal of the Al layer from the MAX phase, and formed stacked MXene sheets. Notably, both 25C and 80C MXene flakes exhibited lamellar structures with lateral dimensions of approximately 5 µm. Both 25C and 80C appeared as evenly formed 2D nanostructured materials with a smooth surface, which offers a large surface-to-volume ratio; materials with these unique morphologies can have novel chemical or physical properties, particularly when these structures fall within the nanoscale scale [31]. On the other hand, the 25C MXene reveals a higher concentration of MAX phase particle residue than 80C MXene nanoparticles. As Fig. 3(b) highlights, the distinctive architecture of residual MAX phase particles was more evident in the 25C sample, hinting at a lower purity level than that of the 80C MXene; furthermore, this observation aligned with the conclusions drawn from the XRD results.

3.2. Particle size dispersion by DLS and imaging techniques

The dispersion characteristics of the MXene were conducted using Dynamic Light Scattering (DLS) by identifying the size distribution of the nanoparticles, and the results are presented in Fig. 4(a). The dispersion level of nanoparticles is a critical factor as it significantly influences the properties of the developed nanocomposite. As presented in the results of DLS particle size analysis, both of the 25C and 80C MXene have a size range between 10^2 to 10^5 nm, and most of the particles around 10^3 to 10^4, which confirmed the observations in FESEM images (Fig. 4(b) and (c)).

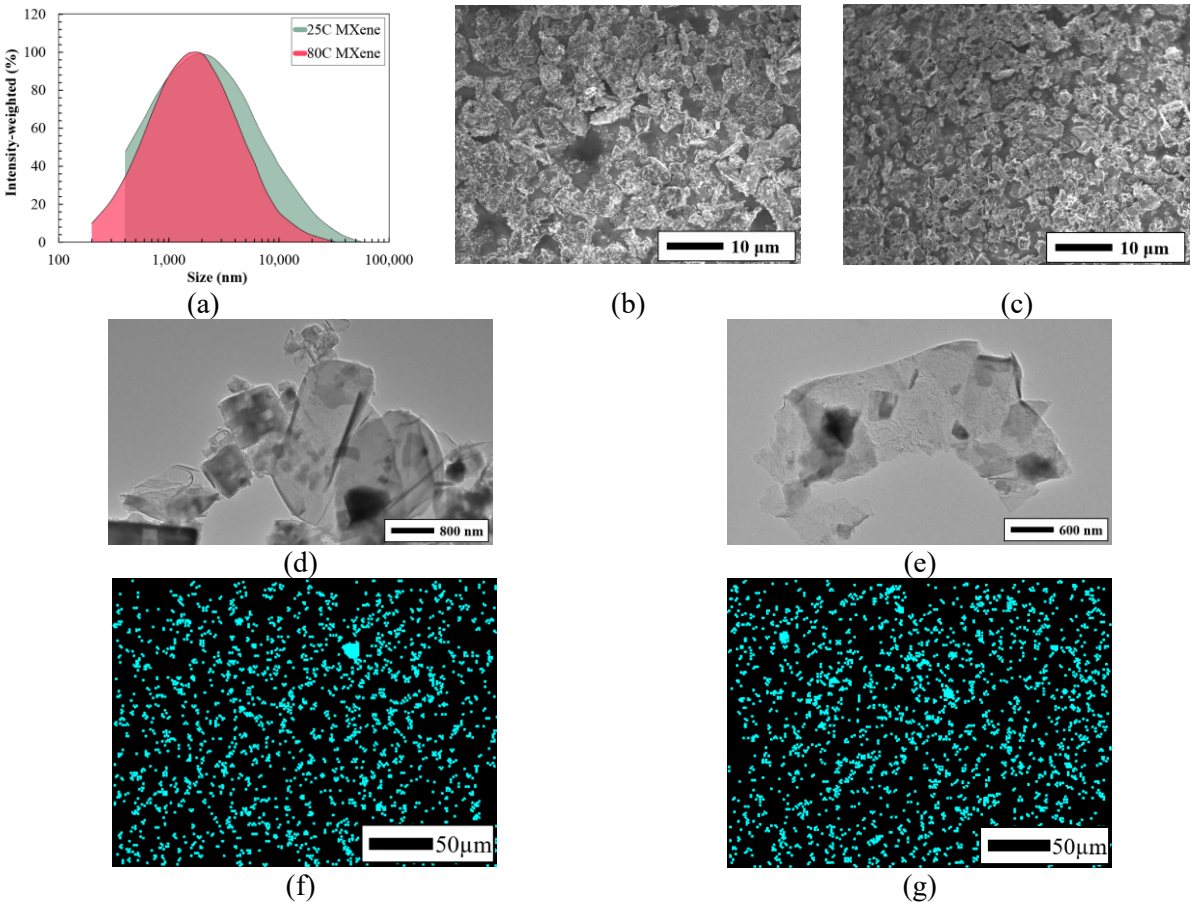

Figure 4. (a) Particle size distribution of 25C and 80C MXene. SEM images of (b) 25C MXene particles and (b) 80C particles. TEM images of (d) 25C and (e) 80C MXene nanosheets after ultrasonication. EDS images of a fracture surface of epoxy reinforced by (f) 25C and (g) 80C MXene.

However, it is worth noting that the 80C MXene nanosheets were generally smaller in size than the 25C MXene, and the mean diameter of the 80C is around 2,600 nm while it is 4,000 nm for 25C. Additionally, the maximum diameter of 25C reached 40,000 nm while the maximum diameter of 80C is 30,000 nm. This finding can be attributed to the higher amount of MAX phase residuals in 25C MXenes which led to a higher tendency to form large agglomerates. Additionally, the smallest size of both 25C and 80C showed a good agreement, as the minimal particles in 80C reached 200 nm, while the minimal particles in 25C was 400 nm. Field Emission Scanning Electron Microscopy (FESEM) findings reinforced the results from Dynamic Light Scattering (DLS) particle size distribution. Fig. 4(c) shows the 80C sample having smaller particles and a higher level of homogeneity compared to the 25C sample. Generally, the smaller and well-distributed nanoparticles improve dispersion and enhance the properties of composites. However, poor nanoparticle dispersion can lead to agglomerations, impacting the material's overall performance.

The MXene particles that were subjected to ultrasonication were also investigated by TEM, as presented in Fig. 4(d) and (e). The observations revealed that ultrasonication successfully separated stacked MXene nanosheets into ultrathin flakes with large surface areas, enhancing dispersion and reducing agglomeration risks. The 80C sample exhibited better dispersion with fewer residuals and thinner layers than the 25C sample, which was likely due to fewer MAX phase particle residuals as indicated by X-ray Diffraction (XRD) and SEM analyses (Fig. 3).

The Energy-dispersive X-ray Spectroscopy (EDS) images in Fig. 4(f) and (g) presented for the 25C and 80C MXene samples in epoxy show distinct differences in particle distribution, which align with previous observations from XRD and SEM analyses. The first image, representing the EDS of 25C MXene in epoxy, reveals a less uniform distribution with a tendency towards larger particle agglomerations. This is consistent with the SEM images and XRD data that indicated a lower crystallinity and purity for the 25C MXene. The presence of larger agglomerates could be indicative of incomplete etching, as also suggested by the XRD analysis, which revealed the presence of TiC impurities and other residual phases from the MAX phase. In contrast, in the EDS image of 80C MXene in epoxy, where the particles are more finely dispersed throughout the matrix. This finer dispersion supports the XRD findings of a more crystalline structure and higher purity for the MXene synthesized at 80°C. A uniform dispersion is often correlated with smaller particle sizes and a more complete etching process, which removes impurities and results in a purer MXene product, as the XRD peaks suggested.

The results of this study elucidate the contrasting dispersion behaviors and subsequent impacts of two distinct types of MXene nanoparticles, labeled as 25C and 80C, which are synthesized under different conditions to yield varying particle morphologies and sizes. The 25C MXene, synthesized using a less intensive processing method, exhibits a coarser morphology with larger and less uniform particles. This morphology leads to heterogeneous dispersion within the epoxy matrix, resulting in areas where the matrix is not uniformly reinforced. Such inconsistencies can adversely affect the mechanical properties of the composite, potentially increase its porosity, and lead to agglomeration. Additionally, the presence of TiC impurities in 25C contributes to these dispersion challenges, further complicating the integration of these nanoparticles into the epoxy matrix. On the contrast, 80C MXene nanoparticles are synthesized under conditions that foster a finer particle size and more uniform morphology. This refined synthesis results in a more even dispersion throughout the epoxy matrix,

297 which is crucial for achieving consistent material behavior across the composite. The uniform dispersion of 80C
298 MXene will improve the interaction between the nanoparticles and the matrix, and the finer particles of 80C
299 contribute to a denser packing within the matrix, significantly reducing porosity and enhancing the barrier
300 properties of the coating.

301 The comparison between these two images highlights the significant effect that synthesis conditions have
302 on the quality and distribution of MXene particles within an epoxy matrix. The 80C MXene's finer dispersion
303 is likely to contribute to a more consistent reinforcement in the composite, potentially leading to better
304 properties and a more reliable performance in practical applications.

305 ***3.3. Influence of the MXene on the microstructure of the nanocomposites***

306 Micro-computed tomography (Micro-CT) is a non-destructive detection method, that provides detailed
307 information into a composite material's internal structure by using cross-sectional X-ray images; the obtained
308 images can be used to identify voids or flaws within the composite. Voids are major defects in nanocomposites
309 and are commonly found in the polymeric composite matrix. These micro-pores form during the mixing and
310 application process, where the viscous polymeric resin restricts the air release process [32]. Consequently, these
311 produced voids could be large enough to degrade the performance of coating, for example, reduce the barrier
312 properties and accelerate damage development. The interaction between the nanofiller and polymer can lead to
313 either a reduction or an increase in voids; therefore, it is crucial to assess the impact of incorporating MXene
314 on the microstructure of the nanocomposite [33–35].

315 As presented in Fig. 5 and 6, the investigations through Micro-CT scanning on pure epoxy and MXene-
316 epoxy nanocomposites demonstrated intriguing findings regarding the effect of MXene concentration on the
317 voids within the composites. In Fig. 5, the pure epoxy sample revealed nonporous microstructures with low
318 void content; however, these voids were notably large in size. This large void formation in epoxy networks
319 could be attributed to the reduced air release due to the epoxy's viscosity during mixing. Therefore, the large
320 voids can be detrimental to the integrity of the composite, as they may reduce the barrier properties, initiate
321 stress concentrations, and potentially lead to material failure for both coatings and substrates when exposed to
322 corrosive conditions.

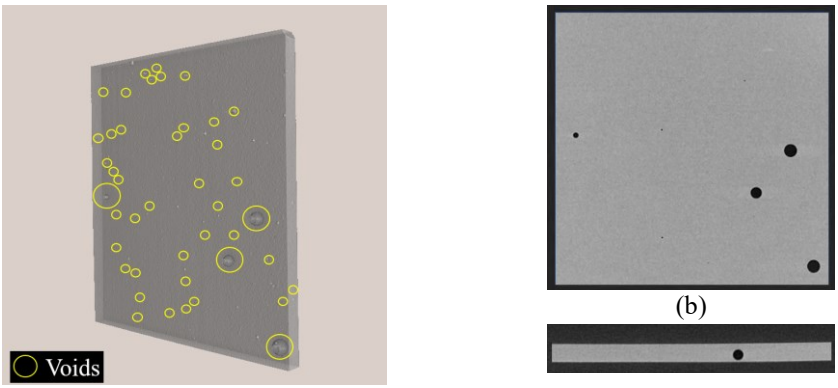

Figure 5. Micro-CT images of neat epoxy (a) transparent 3-D image with areas containing voids highlighted, (b) (c) cross-sectional images.

323

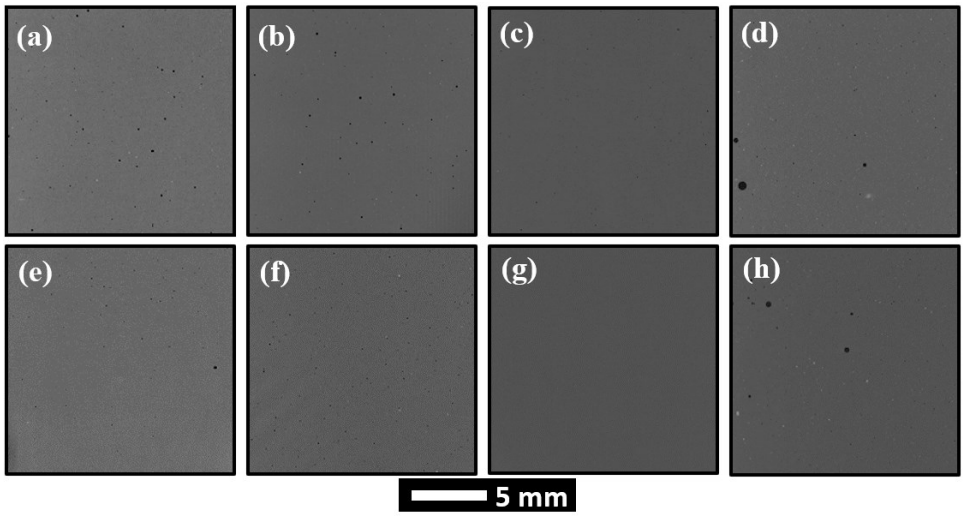

Figure 6. Cross-sectional images of MXene epoxy obtained by Micro-CT, (a) to (d) samples with 25C MXene at 0.1, 0.5, 1.0 and 2.0 wt.%. (e) to (h) samples with 80C MXene at 0.1, 0.5, 1.0 and 2.0 wt.%.

324

325 The incorporation of MXene into the epoxy matrix was found to significantly diminish both the size and
326 numbers of the voids in the MXene-epoxy nanocomposite, implying a beneficial interaction between the MXene
327 and the epoxy matrix. The void reduction for samples confirms the incorporation of both 25C and 80C MXene,
328 improving microstructural integrity by filling in the voids and creating a more continuous, uniform structure,
329 especially for the sample with 0.1% to 1.0% of MXene flakes. However, an interesting trend is observed at
330 higher MXene concentrations, as the samples with 2.0% MXene showed an increase in both void size and
331 amount, which is likely attributable to the elevated viscosity and agglomeration at higher nanofiller contents.
332 This finding emphasizes that the proper amount of MXene can enhance material properties by reducing defects;
333 excessive addition of nanoparticles can lead to the opposite effect.

The results also indicated a slight superiority in void mitigation for 80C MXene-epoxy samples compared to the ones with 25C MXene. This observation showed good agreement with the previous findings that 80C MXene is more exfoliated, which could influence the dispersion of MXene in the epoxy matrix, thus affecting the void formation. Overall, these findings contribute significantly to the understanding of defect formation in MXene-epoxy nanocomposites, and the results are essential for the optimization of nanocomposite performance through defect control.

3.4. Corrosion resistance and durability of the MXene-epoxy nanocomposites

As one of the most common and effective methods to evaluate the coating corrosion protection ability, Electrochemical Impedance Spectroscopy (EIS) measurement was employed to identify the barrier properties of the developed MXene-epoxy coatings before and after exposure to a corrosive environment. In Fig. 7, the impedance and phase angle plots for the steel substrates coated with MXene-epoxy coatings at their initial stage are illustrated, while the results after 250 and 500 hours of salt spray exposure are presented in Fig. 8. The impedance modulus at the low-frequency region (usually 0.01 Hz) in the Bode plots can be used to evaluate the corrosion barrier properties of the coatings [36,37]. Furthermore, the phase angle is a vital parameter for assessing the integrity of corrosion protection coatings. Ideally, the phase angles for an intact coating would approach 90 degrees over a wide frequency range, and a reduction in the phase angle value along with an increase in the corresponding frequency suggests the development of coating delamination [38,39].

Initially, although the impedance value log|Z| at 0.01 Hz was high (above 10), the data collected suggested that the neat epoxy coating was inadequate for providing effective corrosion protection, as evidenced by the noticeable bend in the phase angle curve at the low-frequency range. On the other hand, both 25C and 80C MXene at concentrations of 0.1, 0.5, 1.0, and 2.0 weight percent exhibited high impedance values at the 0.01 Hz point, with log|Z| values exceeding 10. Furthermore, the impedance curves of all the MXene-epoxy coatings were linear, with phase angle values closely approaching 90 degrees across all tested frequencies. This observation indicates that all the MXene-epoxy coating films acted as intact protective layers for the underlying substrates, regardless of the type and concentration of MXene particles. In summary, the obtained results demonstrate that improved corrosion resistance was offered by the addition of both 25C and 80C MXene. The enhanced performance is proved by the high impedance values and near 90 degrees of phase angle values in the collect Bode plots.

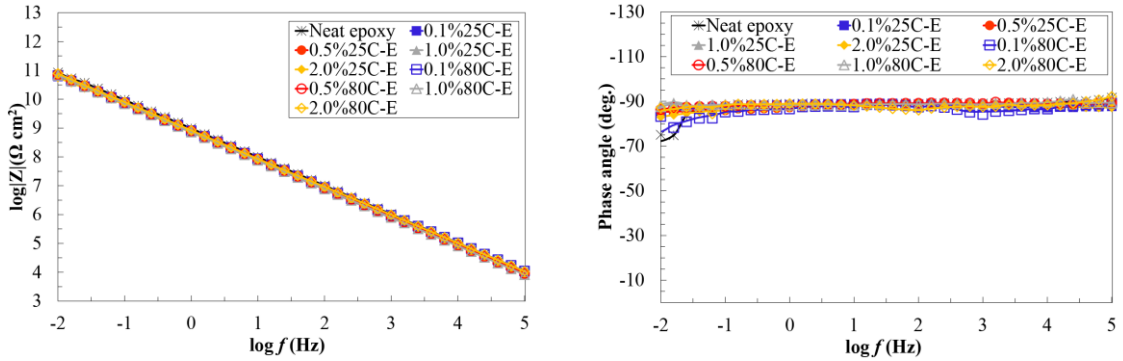

(a) (b)

Figure 7. Bode plots of the MXene-epoxy coatings at the initial stage, (a) impedance plot, and (b) phase angle plot.

As presented in Fig. 8, the long-term corrosion resistance of the neat epoxy coating aligned with previously predicted protection performance. The EIS data obtained after exposure to salt spray for 250 and 500 hours suggested a significant decline in the corrosion protection properties of the neat epoxy coating. As exposure duration increased under the accelerated salt spray durability test, the impedance value at the low-frequency region decreased substantially. The initial value of impedance (log|Z|) was above 10, which dropped to 7.9 after 250 hours and further reduced to 5.3 after 500 hours of exposure, indicating a significant reduction in the coating's barrier properties. Consequently, the minimum region in the phase angle diagram shifts toward higher frequencies, suggesting the barrier performance of the pure epoxy coating degrades under accelerated environmental attacks.

On the other hand, the results highlight the reinforcement of MXene addition on the corrosion resistance of epoxy coatings after exposure to salt spray. The impedance values at 0.01 Hz for both 25C and 80C MXene-epoxy samples generally increased with the concentration of MXene, and these values were higher than the neat epoxy coating at both 250 and 500 hours of exposure. More importantly, the MXene nanocomposite coatings containing 1.0 wt.% MXene showcased the greatest improvement, with no apparent changes in impedance and phase angle. Although material degradation was detected in the other sample groups, their corrosion resistance still surpassed that of the unmodified epoxy. This suggested that the incorporation of both types of MXene nanoparticles, especially with 1.0 wt.%, enhances the corrosion protection performance of epoxy coatings over time, as demonstrated by the improved impedance values in the EIS tests.

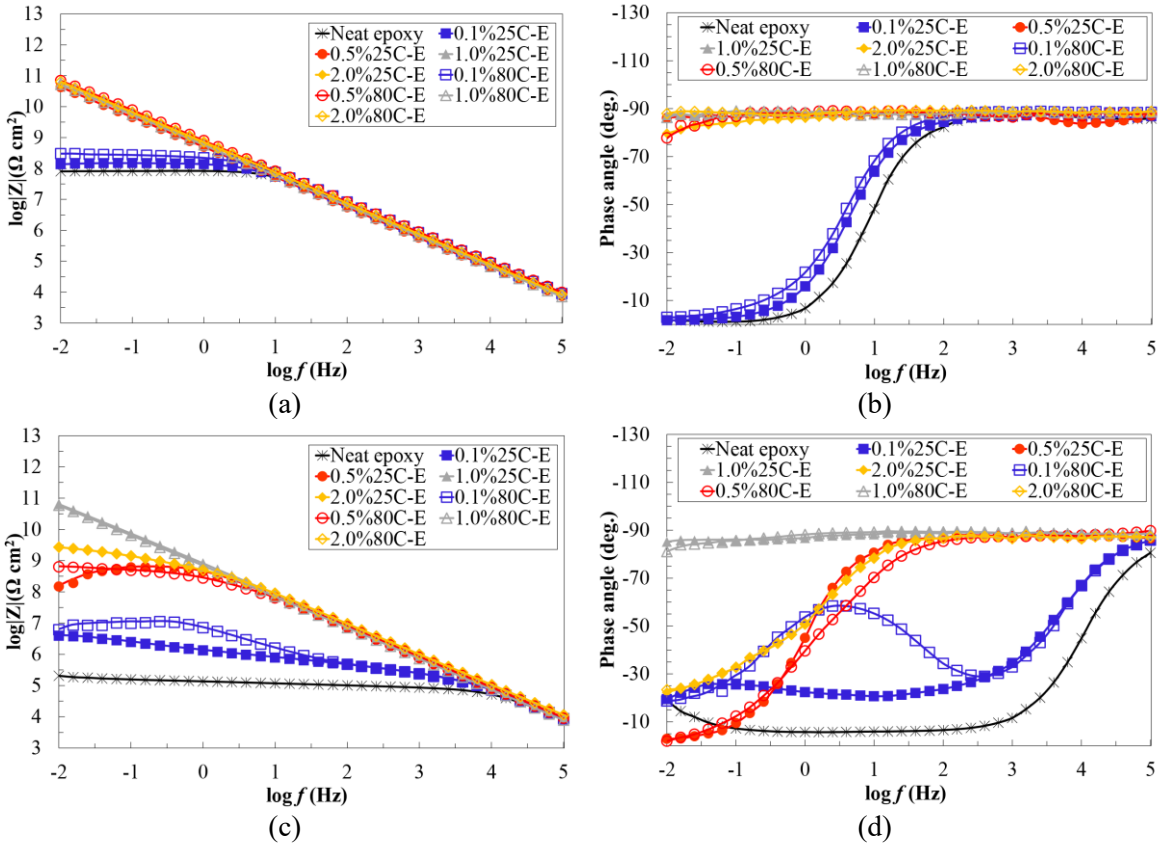

Figure 8. Bode plots of the MXene-epoxy coatings after exposure, (a) impedance plot after 250 hours, (b) phase angle plot after 250 hours, (c) impedance plot after 500 hours, (d) phase angle plot after 500 hours.

The effects of MXene concentration on the corrosion resistance of epoxy coatings can be conducted by considering various mechanisms. The unique two-dimensional structure of MXene nanoparticles contributes to the development of a complex, tortuous pathway throughout the coating to the substrate. This tortuous pathway hinders the penetration of corrosive agents through the coating and reduces the rate for them to reach the substrate. This phenomenon may explain the increased impedance values observed when incorporating MXene nanoparticles into the epoxy. Additionally, the presence of MXene nanoparticles can enhance the coating by creating a composite material with fewer and smaller pores or defects, thereby inhibiting the infiltration of corrosive substances. This improvement might be due to MXene's ability to reduce voids in the composite, which was observed in Micro-CT test. The improved corrosion resistance associated with increasing MXene concentrations, up to 1.0% for both 25C and 80C MXene-epoxy specimens, supported this assumption. On the other hand, when the MXene concentrations increased, such as 2.0%, corrosion resistance appeared to decline compared to samples containing lower concentrations of MXene (1.0%). This reduction might be attributed to

the formation of large-sized agglomerates and voids within the coating, which function as defects and assist the penetration of corrosive media.

In summary, both 25C and 80C MXene enhance corrosion resistance compared to the neat epoxy, with the 80C MXene-epoxy samples generally exhibiting slightly superior performance. The findings suggested that an optimal MXene concentration exists for maximizing corrosion resistance, potentially attributable to the balance between the advantageous effects of MXene's 2-D structure and reduced voids.

3.5. Evaluation of corrosion damages over time using EEC modeling

The electrochemical equivalent circuit (EEC) model, comprising a finite set of elementary (resistors, capacitors, and inductors), is generalized to match the collected EIS data, so the corrosion stage of the coating-substrate system can be characterized. The electrical equivalent circuit (EEC) model is a mathematical model that represents the corrosion process of a coated metal as an electrical circuit. In the EEC model, the coated metal is represented by a series combination of an electrical resistor and a capacitor. In order to assess the coating deterioration under increased environmental stress, four types of EEC models are generally incorporated to characterize the corrosion stage. As depicted in Fig. 9, from Model A to Model C, the state of the coating system ranges from undamaged to severely corroded.

Model A describes the coatings remaining intact in the initial stage (Stage I), and the EEC model is constructed by solution resistance (R_{sol}), coating resistance (R_c), and constant-phase element of the coating (CPE_{po}). Model B examines the coating with imperfections, in which the electrodes being able to break through the polymer film and contact the metallic surface, therefore triggering corrosion in the substrate. Under this scenario, the corrosion activity is in Stage II; hence, charge transfer resistance (R_{ct}) and constant-phase element of double-charge (CPE_{dl}) should be introduced to model the corrosion behaviors at the occurs at the coating-substrate interface. In the third phase, corrosion products diffuse via coating defects, and this activity begins to predominate the corrosion reaction in the coated system. Therefore, the Warburg diffusion element (W_s) is adopted to the EEC model in order to clarify the diffusion effect, which denotes that the corrosion process has reached Stage III. Model C is employed to represent coating systems that under severe corrosion damage, suggesting that a thin layer of rust has formed in the coating-substrate interface. In order to simulate the layer of corrosion products, constant phase element of diffusion capacitance (CPE_{diff}) and diffusion resistance (R_{diff}) are substituted for Warburg diffusion at this stage (Stage IV).

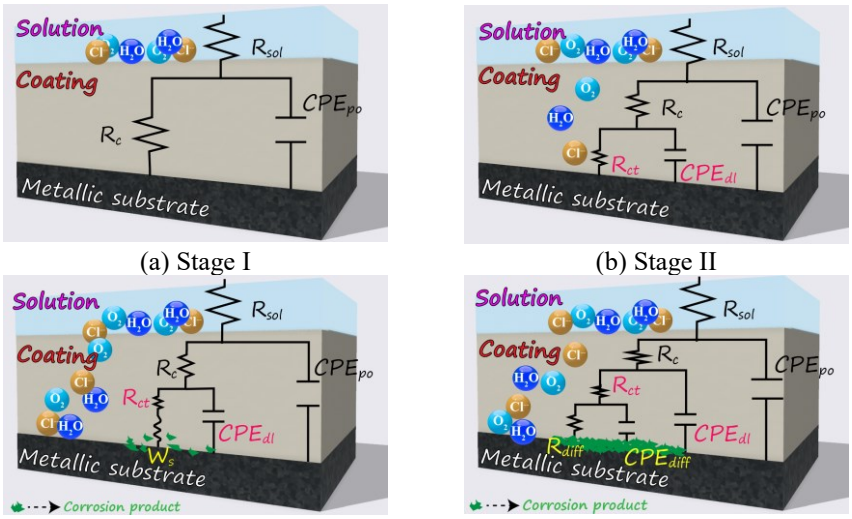

(a) Stage I (b) Stage II

(c) Stage III (d) Stage IV

Figure 9. EEC model for each corrosion stage.

The following discussion expands on the corrosion stages of each developed MXene nanocomposite coatings, providing a more detailed analysis of their performance under B117 salt spray exposure, and the results are summarized in Table 1. The neat epoxy sample exhibited a rapid progression in corrosion stages, starting at Stage II at the onset and reaching Stage IV after 500 hours of exposure. This finding indicated that the coating had imperfections, which allowed the electrodes to encounter the metallic surface, leading to corrosion in the substrate. The progression to Stage IV after 500 hours demonstrates that a thin layer of rust had formed at the coating-substrate interface, further weakening the protective properties of the coating.

Table 1. The corrosion stage of MXene-epoxy coated samples after exposure.

Label	Corrosion stage determined by EEC model		
	Onset	250-hr	500-hr
Neat epoxy	Stage II	Stage II	Stage IV
0.1%25C-E	Stage I	Stage III	Stage III
0.5%25C-E	Stage I	Stage I	Stage II
1.0%25C-E	Stage I	Stage I	Stage I
2.0%25C-E	Stage I	Stage II	Stage III
0.1%80C-E	Stage I	Stage III	Stage III
0.5%80C-E	Stage I	Stage I	Stage II
1.0%80C-E	Stage I	Stage I	Stage I
2.0%80C-E	Stage I	Stage II	Stage III

Results from the corrosion stage analysis indicated that both 25C and 80C MXene have shown extraordinary improvement in corrosion resistance. The samples containing 0.1% of 25C MXene and 80C MXene, started at Stage I and transitioned to Stage III after 250 hours of exposure. This suggests that the

coatings initially remained intact but later developed imperfections, allowing corrosion products to diffuse through the coating defects. The samples remained at Stage III even after 500 hours, indicating that the corrosion process was dominated by the diffusion of corrosion products at this stage.

The samples with 0.5% MXene loading (0.5%25C-E and 0.5%80C-E) exhibited improved corrosion resistance compared to the 0.1% loaded samples, as they remained at Stage I after 250 hours of exposure, demonstrating that the coatings were still intact and providing effective protection to the metal substrate. After 500 hours, these samples progressed to Stage II, suggesting that some corrosion damage had developed in the coating-substrate interface. The samples with 1.0% MXene loading (1.0%25C-E and 1.0%80C-E) showed the most stable corrosion resistance throughout the test period, remaining at Stage I even after 500 hours of exposure. This highlights the superior performance of these coatings, as they maintained their effective protection properties and prevented corrosion in the metal substrate. On the other hand, the samples with 2.0% MXene loading (2.0%25C-E and 2.0%80C-E) initially exhibited Stage I corrosion resistance; however, they progressed to Stage II after 250 hours of exposure and reached Stage III after 500 hours. The observations from 2.0%25C-E and 2.0%80C-E samples indicated that while the higher MXene loading provided initial protection, the voids and imperfections in coatings eventually allowed corrosive media and corrosion products to diffuse through the defects.

The observations from the images presented in Fig. 10 are in firm agreement with the EIS and EEC results. The images in Fig. 10 presented the coated samples after 250 and 500 hours of B117 salt spray exposure. In the case of pure epoxy, corrosion products began accumulating from 250 hours of exposure, and after 500 hours, these products penetrated the coating and reached the top surface.

Epoxy samples containing 25C and 80C MXene exhibited similar observations, and corrosion reactions were noted in both samples containing 0.1% and 2.0% MXene. However, the corresponding mechanisms are different: for the 0.1% MXene samples, the lower concentration of MXene could not provide strong reinforcement against corrosion. In contrast, for the 2.0% MXene samples, the large amount of MXene created agglomerates and voids, leading to accelerated corrosion damages. Consequently, the corrosion type in 0.1% MXene samples was general corrosion, while in 2.0% samples, it was localized in defective areas. In the case of the 2.0% MXene samples, the EIS results at 250 hours indicated that the coatings exhibited excellent barrier properties. However, some coating damage was observed in areas with large MXene agglomerates; as a result,

these agglomerated spots developed into localized corrosion after 500 hours of salt spray exposure. The interaction between the MXene agglomerates and the epoxy matrix could play a role in this localized coating degradation. The larger MXene agglomerates might disrupt the uniformity of the epoxy matrix, creating weak spots that are more susceptible to corrosive attacks. These weak spots could lead to a higher concentration of stress, allowing the penetration of corrosive species and accelerating the corrosion process.

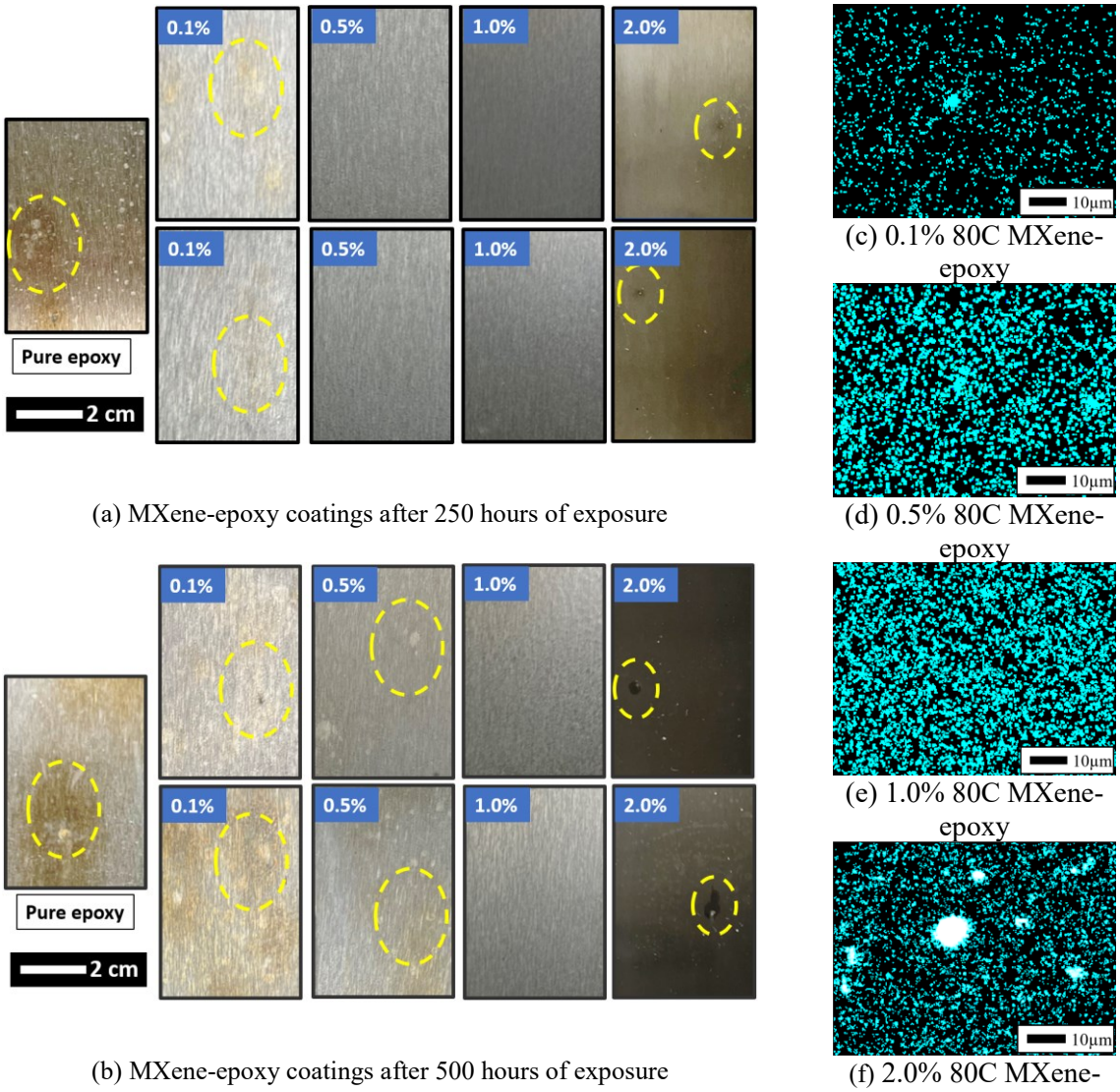

(a) MXene-epoxy coatings after 250 hours of exposure

(b) MXene-epoxy coatings after 500 hours of exposure

(c) 0.1% 80C MXene-epoxy

(d) 0.5% 80C MXene-epoxy

(e) 1.0% 80C MXene-epoxy

(f) 2.0% 80C MXene-epoxy

Figure 10. Images of MXene-epoxy coatings after salt spray exposure, (a) 250 hours and (b) 500 hours. EDS images (c) to (f) of cross-sectional surface for MXene-epoxy nanocomposite.

Meanwhile, the 0.5% MXene samples demonstrated improved corrosion resistance due to the increased amount of MXene; however, corrosion production and coating delamination were still observed after 500 hours. In comparison, the 1.0% MXene samples showed the most substantial improvement in corrosion resistance,

with no corrosion reactions detected after 500 hours. Thus, the observations from the images are in strong agreement with the EIS results and the corrosion stage in Table 1.

To further study the mechanism of corrosion protection behavior, the sequence of Energy-dispersive X-ray Spectroscopy (EDS) images (Fig. 10 (c) to (f)) were used to depicts the cross-sectional-surface of epoxy composites containing 80C MXene at varying concentrations: 0.1%, 0.5%, 1.0%, and 2.0%. An analysis of these images reveals critical insights into the dispersion behavior of MXene within the epoxy matrix and its subsequent impact on the material's anti-corrosive properties. At the 0.1% MXene concentration, the EDS micrographs reveal a sparse distribution of MXene particles within the epoxy matrix. While some degree of MXene presence is evident, there exist extensive regions within the matrix that lack MXene coverage, potentially resulting in insufficient reinforcement against corrosive media. As the concentration increases to 0.5% and 1.0%, there is a notable increase in particle density, yet the dispersion remains relatively even. This homogeneity is beneficial for corrosion protection as it allows for a consistent protective layer that can prevent corrosive elements from reaching the underlying material. However, in Fig. 10(f), at the highest concentration of 2.0%, areas of agglomeration were found where MXene particles have clustered together. These agglomerates could potentially create weak points in the composite material, which may negatively impact corrosion resistance. Agglomerates act as barriers to uniform stress distribution and can be sites where corrosion initiates and propagates more easily due to the less protected epoxy regions around them.

The increasing density of MXene particles up to 1.0% likely contributes to improved barrier properties of the epoxy composite, as the particles create a tortuous path for corrosive agents, thus enhancing the corrosion protection performance. However, the excessive agglomeration observed at 2.0% could compromise this protective effect due to the formation of non-uniform layers that are less effective at impeding corrosion. In summary, the EDS images show that while increasing the MXene content up to a point can enhance the composite's protective qualities against corrosion, over-saturation leads to agglomeration, which can have the opposite effect. The optimal concentration for corrosion protection likely lies at or below 1.0%, where the benefits of MXene addition are maximized without the drawbacks of particle clustering.

3.6. Evaluation of coating degradation over time using coating protection index

To simplify the evaluation of coating's performance degradation process in a severely corrosive environment, two types of damage indices were employed; both were modified depending on those

implemented by previous studies [40]. As presented in Fig. 11, both type I and II coating damage indices were derived by interpreting the impedance curves in Bode plots.

In the impedance plot of a coating that functions as an intact protective barrier, as depicted in Fig. 11, the slope of the impedance curve will retain -1, and the plot will contain solely capacitive areas. Alternatively, if the protective film begins to deteriorate or experience damage, the slope of the impedance curve will drop, especially in low frequency ranges, as seen in Fig. 11.

As illustrated in the equation (1), the first damage index (DI_1) was calculated by the change of Zmod values measured at the lowest frequencies, in this case 0.01 Hz, after coating degradation.

$$DI_1(\%) = \left(\frac{Log\ Z_{damaged}}{Log\ Z_{intact}}\right) * 100 \quad (1)$$

where, Z_{intact} and Z_{damage} represent impedance values ($Z_{0.01Hz}$) at the intact and damaged stages, accordingly.

The other damage index (DI_2), in equation (2), is derived from the capacitive and resistive areas of the bode plot, which reflects the degradation of coating performance over the whole frequency range that tested:

$$DI_2(\%) = \left(\frac{A_1+A_2}{A_1+A_2+A_3}\right) * 100 \quad (2)$$

whereby the region under the impendence slope is subdivided into capacitive (A2) and resistive (A1) areas according to the threshold frequency values at -45° phase angle [41,42]. As soon as the electrolyte solution penetrates the coated specimens, coating degradation and corrosion at the coating-substrate interface will be initiated. In this situation, the impedance curve will respond by decreasing capacitive region and expanding the resistive region [43]. Consequently, the impedance curve will include both a resistive region and a capacitive region, and an additional area (A3) could be identified just above the resistive region (A1) for the damaged coating, compared to an undamaged coating. For both damage indices, the greater the index value, the less the coating degrades. Therefore, a sample with an index value of 100 percent, for instance, suggests that the coated film serves almost as an isolating layer to protect the substrate.

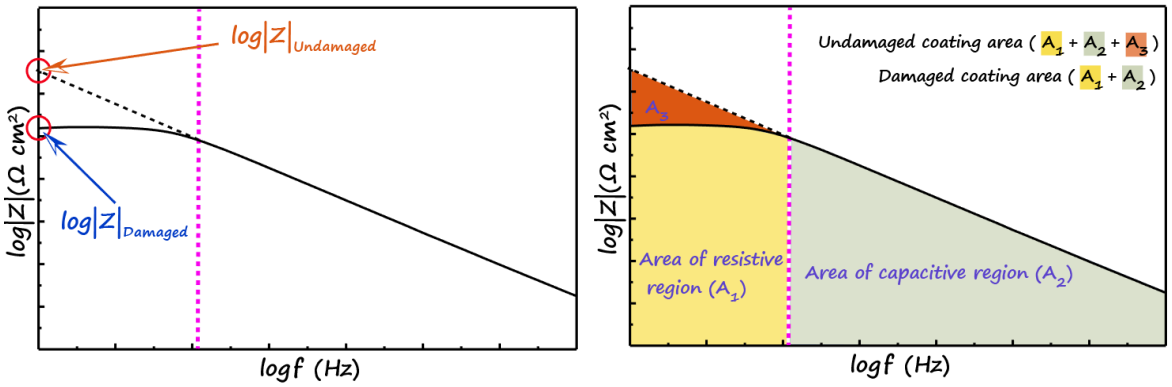

(a) (b)

Figure 11. Damage index for the coating degradation assessment: (a)-(b), (c)-(d)

The findings from damage index I and II offer valuable insights into the performance and durability of MXene-epoxy coatings when exposed to a corrosive environment (Fig. 12). Damage index I results demonstrate that coatings containing higher MXene concentrations (1.0% and 0.5%) exhibit improved durability and corrosion resistance, even after 500 hours of exposure. Notably, the 1.0%25C-E coating retains 99% of its initial performance after 500 hours, while the 0.5%25C-E coating maintains 82%. These findings align with the EEC model and EIS data, which suggest that these coatings possess enhanced barrier properties and heightened corrosion resistance. The 1.0%80C-E coating, in particular, retains its full initial performance after 500 hours, illustrating its exceptional resilience in a corrosive environment.

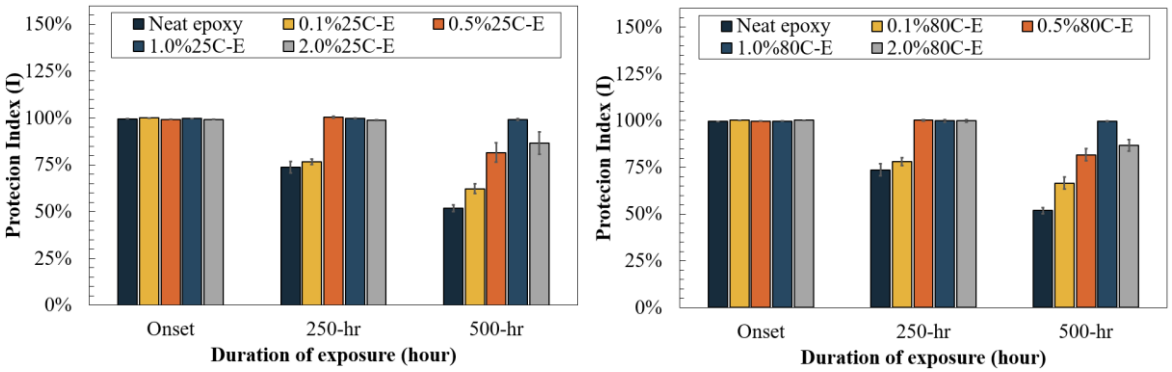

(a) (b)

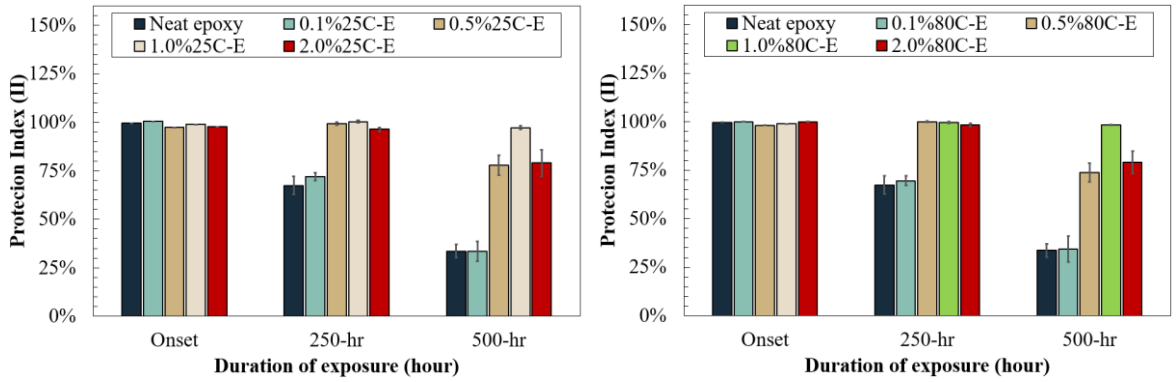

Figure 12. Protection indices of epoxy composites reinforced by (a) 25C and (b) 80C MXene.

Similar findings were observed in damage index II, and results indicate that coatings with lower MXene concentrations (0.1%25C-E and 0.1%80C-E) and neat epoxy experience substantial degradation over time. After 500 hours, the performance of these coatings drops significantly, with neat epoxy retaining only 34% of its initial performance, 0.1%25C-E at 33%, and 0.1%80C-E at 34%. These observations correspond with the EIS data, which shows that lower MXene concentrations and neat epoxy coatings exhibit increased corrosion rates, reduced coating resistance, and progression through various corrosion stages.

It is crucial to note that while 2.0% MXene coatings display relatively high durability, their performance declines after 500 hours due to the presence of large agglomerates within the coating. The 2.0%25C-E and 2.0%80C-E coatings retain above 80% of their initial performance at both damage indices, respectively. This finding is supported by Micro-CT images and EIS data, which identify localized corrosion in areas with higher MXene agglomerates.

In summary, the insights from damage indices I and II, combined with the EEC model and EIS data, emphasize the effectiveness of MXene-epoxy coatings in delivering exceptional corrosion resistance and durability. Optimal MXene concentrations (1.0% and 0.5%) provide the best performance, while coatings containing lower MXene concentrations or large agglomerates experience a decline in their protective capabilities over time

3.7. Evaluation of coating performance over time using water absorption analysis

The penetration of water or other active ionic species through thin polymer coatings is a common cause of coating failure. Since the capacitance and resistance of a polymeric film change as it absorbs water, electrochemical impedance spectroscopy (EIS) results provide an estimation of the amount of water uptake in

the polymer [44]. Due to the fact that water's dielectric constant is greater than common polymers, it is anticipated that the absorption of water will raise the capacitance of the coating. Brasher and Kingsbury utilized the model used to estimate the water absorption of a coating, as presented below:

$$\emptyset = \frac{K \log(\frac{C_t}{C_0})}{\log(\varepsilon_w)} \quad (2)$$

where Φ is the water content volume percentage, Ct and C0 are the capacitance of the coating before and after the test, respectively. Additionally, ε_w is the dielectric constant of water at operating temperatures (=78.5 at 25 degrees Celsius and 75 at 35 degrees Celsius).

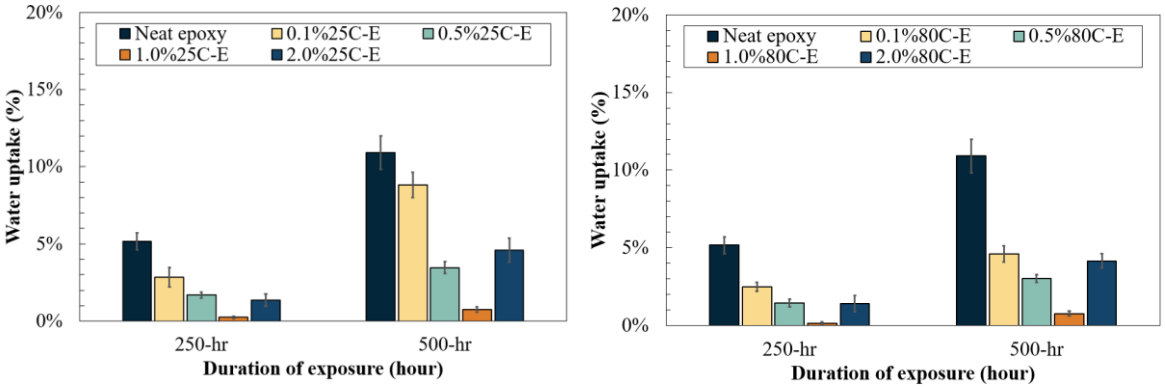

Figure 13. Water uptake of epoxy composites reinforced by (a) 25C and (b) 80C MXene.

The water uptake results after 250 and 500 hours of B117 Salt spray exposure provide valuable information regarding the performance of the MXene-epoxy coatings in resisting water penetration, a common cause of coating failure. The results of the water uptake are presented in Fig. 13. The data reveals that the MXene-epoxy coatings (0.1%, 0.5%, 1.0%, and 2.0%) generally exhibit lower water uptake compared to the neat epoxy. This indicates that the incorporation of MXene into the epoxy matrix improves the resistance of the coatings to water penetration, which is an essential factor in determining the overall performance and durability of protective coatings.

Among the MXene-epoxy coatings, the 1.0%25C-E and 1.0%80C-E samples display the lowest water uptake values, suggesting superior resistance to water penetration. This finding correlates well with the previously discussed damage indices, EEC models, and EIS results, where these coatings exhibited excellent barrier properties and increased corrosion resistance. The lower water uptake values in the MXene-epoxy coatings can be attributed to the MXene particles acting as barriers to water penetration, thus enhancing the

overall performance of the epoxy matrix. Additionally, the water uptake results can also be correlated with the porosity of the MXene-epoxy composite coatings. The addition of MXene into the epoxy matrix has been observed to reduce the porosity and void sizes within the coatings, as evidenced by the Micro-CT images. However, it should be noted that the coatings with higher MXene concentrations (2.0%25C-E and 2.0%80C-E) display a higher water uptake than the coatings with lower MXene concentrations. This may be due to the presence of large agglomerates in the coatings, as discussed earlier, which negatively impact the protective capabilities of the coatings.

In conclusion, the optimal MXene concentrations (1.0% and 0.5%) offer the best performance, whereas the coatings with lower MXene concentrations or large agglomerates show a decline in their protective capabilities over time. The synergistic effects of MXene's barrier properties and the changes in porosity due to its incorporation into the epoxy matrix contribute significantly to the improved performance of MXene-epoxy composite coatings. The barrier properties of MXene are primarily attributed to its high aspect ratio, which forms tortuous pathways for water and other corrosive agents, effectively impeding their penetration through the coating. Simultaneously, the addition of MXene to the epoxy matrix results in a more densely packed composite structure, reducing porosity and void sizes.

3.8. Anti-aging properties of MXene-epoxy nanocomposites

Epoxy resins usually have excellent mechanical properties, chemical resistance, and adhesion, which makes them widely used in various industries. However, environmental conditions such as heat, light, and oxygen can compromise their stability, promoting the generation of free radicals. These highly reactive species with unpaired electrons can cause a chain reaction leading to material degradation. Over time, these radicals can trigger more chemical reactions, causing further degradation of the polymer network. Therefore, it is crucial to minimize free radical formation and preserve the long-term stability and performance of the epoxy resin, and the quantity of free radicals can be used as a measure for the aging/degradation of the epoxy nanocomposite.

The anti-aging capabilities of a coating significantly enhance its corrosion protection in two primary ways; firstly, anti-aging properties in materials, especially those used in coatings, are crucial in reducing the rate of degradation due to environmental factors. These properties help in maintaining the structural integrity of the protective barriers over extended periods [45]. By preventing the breakdown of material structures, anti-aging capabilities ensure that the onset of corrosion, which often follows material weakening or failure, is significantly

delayed. Secondly, as coatings age, they can become more brittle [46]; anti-aging properties play a vital role in preserving the elasticity and mechanical strength of these coatings. This preservation is crucial in preventing the initiation and propagation of micro-cracking, which can occur due to the generation and diffusion of corrosion products. Moreover, maintaining the coating's integrity prevents chipping and ensures that the barrier remains seamless and intact, which is essential for effective long-term corrosion protection.

The anti-aging ability introduced by the addition of MXene is assessed by comparison with pure epoxy samples after exposure. The concentration of free radicals within the system can be estimated via the following equation:

$$I \propto 2Y'_m(\Delta H_{pp})^2 \quad (1)$$

where $2Y'_m$ denotes the peak-to-peak amplitude, ΔH_{pp} symbolizes the width between peaks in the sample spectrum, and I stands for the signal strength [47]. Therefore, the peak-to-peak amplitude ($2Y'_m$) directly associated with the free radical concentration when the peak to peak width is consistent [47]. Therefore, Fig. 14 presents the collected ESR data for all tested samples after 500 hours of exposure to a corrosive environment, and the peak in all the tested samples indicates the presence of hydroxyl (O–H) radicals, which are formed by the aging process of epoxy [48]. In order to simplify comparison, the amplitude to epoxy is assigned as 100% as a standard, with other samples computed as percentages accordingly.

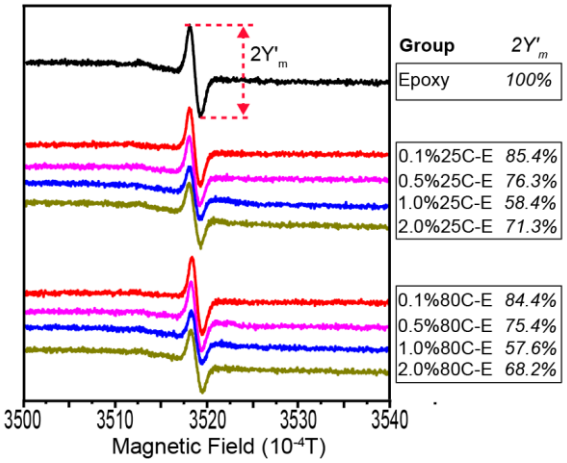

Figure 14. ESR spectra measurement of samples after exposure to corrosive environment.

As presented in Fig, 14, the spectrum of all the tested samples showed a simple curve with one central peak which might be the presence of free radicals that formed due to the aging process of the epoxy [48]. The collected data indicated neat epoxy demonstrated the highest intensity of these free radicals, indicating its aging susceptibility in a corrosive environment. However, the addition of Mxene to the epoxy matrix brought a

significant reduction in free radical generation. For both 25C and 80C Mxene-epoxy groups, there was a clear trend of diminishing free radical intensity with increasing Mxene concentration up to 1.0%. This observation aligned well with the concept that nanofillers like Mxene improved microstructural stability, as well as enhanced anti-corrosion properties of the composite material. More specifically, MXene appeared to mitigate the epoxy aging process under corrosive conditions by suppressing radical generation. However, at the highest Mxene concentration (2.0%) an increase in free radical intensity was observed. This finding highlights the previous conclusion in the discussion of Micro-CT results, in which excessive concentrations of MXene nanoparticles potentially lead to defects and agglomerations within the composite. In this case, the structural irregularities could facilitate oxygen diffusion into the coating, triggering a more rapid reaction of carbon radicals with atmospheric oxygen, leading to accelerated degradation [47].

The results showed a good agreement with previous microstructural, EIS, and EDS imaging analyses, offering a more holistic picture of the effects of Mxene reinforcement in epoxy-based nanocomposites. Especially with the EDS data (Fig. 10 (c) to (f)), at a 0.1% concentration of MXene, the lower concentration might contribute to a certain degree of aging resistance by interrupting the pathway of UV radiation and other aging agents, the insufficient coverage by MXene particles likely leads to areas within the matrix that remain unprotected. This could allow for oxidative and UV-induced degradation processes to occur more readily in those regions, potentially compromising the composite's overall anti-aging performance. Higher concentrations (0.5 and 1.0%) improve this protective effect by providing more uniform coverage. However, at 2.0% MXene, particle agglomerations might compromise the composite's anti-aging performance by creating localized weak points vulnerable to faster degradation. Thus, an optimal MXene concentration exists that maximizes aging resistance without the negative impact of particle clumping. The comprehensive study underscores the multifaceted improvements when incorporating MXene into the composite, not only in terms of microstructural enhancements and anti-corrosion characteristics but also in aging resistance.

4. Conclusion

In summary, two fabrication methods were used to develop lamellar $Ti_3C_2T_x$ MXene nanoparticles, a 2D graphene-like nanomaterial, labeled as 25C and 80C, and novel MXene-epoxy nanocomposite coatings were successfully synthesized. The application of using MXene as reinforcement was introduced into epoxy resin to fabricate high-performance protection coating with extraordinary robustness. The fabricated MXene and

MXene-based nanocomposite coatings were characterized by XRD, SEM, and TEM measurements to investigate structure, morphology, and composition. Both the MXene-reinforced epoxy coating systems were prepared with the varied contents of MXene nanofillers, ranging from 0.1 to 2.0 wt.%, and the major findings were summarized based on experimental results:

- A comparison between the 25C and 80C variants of MXene highlights that the finer morphology and better dispersion of MXene generated at 80C lead to enhanced performance of the composite material. This further emphasizes the significance of optimizing the production conditions of MXene to maximize its beneficial contributions to the nanocomposite.
- Both 25C and 80C MXene significantly influenced the microstructure of the epoxy composite, reducing void formation and promoting homogeneity at the microscale. This improved microstructure played a vital role in enhancing the overall performance of MXene-based nanocomposites.
- The results of this study demonstrated the potential of MXene nanoparticles as an effective reinforcement for polymeric coatings, enhancing their corrosion resistance and durability. The superior performance of the 1.0% MXene-loaded samples (1.0%25C-E and 1.0%80C-E) highlights the benefits of incorporating MXene into epoxy matrices, with the coatings maintaining their protective properties even after prolonged exposure to B117 salt spray.
- The findings from the damage indices show that optimal MXene concentrations (1.0% and 0.5%) provide enhanced protection in MXene-epoxy coatings. In contrast, coatings with lower MXene concentrations or those containing large agglomerates experience reduced protective capabilities over time. Water absorption studies also reinforce these observations. MXene's intrinsic barrier properties, attributed to its high aspect ratio that establishes complex pathways, combined with the reduced porosity and void sizes in the epoxy matrix due to its addition, culminate in a highly resistant composite against corrosive agents.
- Significantly, this study established MXene's potential in improving the anti-aging properties of epoxy. By reducing the formation of free radicals and enhancing the corrosion resistance of the composite, MXene has demonstrated its potential as a novel solution for epoxy degradation issues.

In conclusion, this study investigates the integration of $Ti_3C_2T_x$ MXene into epoxy coatings and its potential to bolster anti-corrosion properties through multiple mechanisms. $Ti_3C_2T_x$ MXene significantly enhances the

barrier properties of epoxy coatings due to its high aspect ratio and layered structure. This configuration establishes complex, tortuous pathways for corrosive agents, effectively impeding their penetration and delaying the onset of corrosion processes on the substrate. Micro-CT analysis demonstrates that MXene uniformly disperses within the epoxy matrix, effectively filling voids and reducing defects that could initiate corrosion, thus preserving the integrity of the coating under various conditions. Furthermore, the observed decrease in free radical formation indicates that MXene not only improves the physical and chemical properties but also significantly boosts the oxidative stability of the coatings. This enhancement prolongs the lifespan of materials, as degradation in epoxy typically leads to diminished performance and facilitates the initiation and propagation of microcracks. These attributes collectively contribute to the superior performance of MXene-epoxy composites in corrosive environments, underscoring their potential in extending the application range of these coatings to sectors such as marine, automotive, and aerospace where durability and reliability are critical. Therefore, the discovery in this manuscript provides guidance for designing and exploiting a high-performance MXene reinforced polymeric composites. The incorporation of MXene nanoparticles into epoxy coatings results in a significant improvement in their protective properties, paving the way for the development of advanced, long-lasting, and multifunctional coatings for various applications.

CRediT authorship contribution statement

Xingyu Wang: Conceptualization, Data curation, Investigation, Formal analysis, Methodology, Validation, Writing - original draft, Writing - review & editing. **Sampada Koirala:** Formal analysis, Methodology, Validation, Writing - original draft. **Luyang Xu:** Formal analysis, Methodology, Validation. **Qiaobin Li:** Formal analysis, Methodology, Validation. **Zhibin Lin:** Supervision, Conceptualization, Investigation, Methodology, Validation, Visualization, Writing - review & editing. **Xiaoning Qi**: Formal analysis, Methodology, Validation. **Zhongyu Yang:** Formal analysis, Methodology, Validation**. Ying Huang:** Supervision, Investigation, Writing - review & editing.**, Danling Wang:** Supervision, Conceptualization, Investigation, Methodology, Validation, Visualization, Writing - review & editing.

Declaration of competing interest

The authors declare that they have no known competing financial interests or personal relationships that could have appeared to influence the work reported in this paper.

Acknowledgments

This work was partially supported by the U.S. Department of Transportation PHMSA (Grant No. 693JK32110003POTA, 693JK32250007CAAP, and 693JK3250009CAAP), the National Science Foundation (CMMI-1750316, Eager-2226202, RII Track 2 – 2218046, and RII Track 1 – ND-ACES 1946202), ND NASA EPSCoR, and ND EPSCoR. The results, discussion, and opinions reflected in this paper are those of the authors only and do not necessarily represent those of the sponsors.

Reference

[1] Gong K, Zhou K, Qian X, Shi C, Yu B. MXene as emerging nanofillers for high-performance polymer composites: A review. Composites Part B: Engineering 2021;217:108867.
[2] Li X, Wang C, Cao Y, Wang G. Functional MXene materials: progress of their applications. Chemistry–An Asian Journal 2018;13:2742–57.
[3] Giménez R, Serrano B, San-Miguel V, Cabanelas JC. Recent advances in MXene/epoxy composites: trends and prospects. Polymers 2022;14:1170.
[4] Song P, Qiu H, Wang L, Liu X, Zhang Y, Zhang J, et al. Honeycomb structural rGO-MXene/epoxy nanocomposites for superior electromagnetic interference shielding performance. Sustainable Materials and Technologies 2020;24:e00153.
[5] Gao L, Li C, Huang W, Mei S, Lin H, Ou Q, et al. MXene/polymer membranes: synthesis, properties, and emerging applications. Chemistry of Materials 2020;32:1703–47.
[6] Yang J, Bao W, Jaumaux P, Zhang S, Wang C, Wang G. MXene-based composites: synthesis and applications in rechargeable batteries and supercapacitors. Advanced Materials Interfaces 2019;6:1802004.
[7] Jimmy J, Kandasubramanian B. Mxene functionalized polymer composites: Synthesis and applications. European Polymer Journal 2020;122:109367.
[8] Khazaei M, Arai M, Sasaki T, Chung C-Y, Venkataramanan NS, Estili M, et al. Novel electronic and magnetic properties of two-dimensional transition metal carbides and nitrides. Advanced Functional Materials 2013;23:2185–92.
[9] Habibpour S, Um JG, Jun Y, Bhargava P, Park CB, Yu A. Structural impact of graphene nanoribbon on mechanical properties and anti-corrosion performance of polyurethane nanocomposites. Chemical Engineering Journal 2021;405:126858.
[10] Xue Y, Feng J, Huo S, Song P, Yu B, Liu L, et al. Polyphosphoramide-intercalated MXene for simultaneously enhancing thermal stability, flame retardancy and mechanical properties of polylactide. Chemical Engineering Journal 2020;397:125336.
[11] Aakyiir M, Yu H, Araby S, Ruoyu W, Michelmore A, Meng Q, et al. Electrically and thermally conductive elastomer by using MXene nanosheets with interface modification. Chemical Engineering Journal 2020;397:125439.
[12] Naguib M, Mashtalir O, Carle J, Presser V, Lu J, Hultman L, et al. Two-dimensional transition metal carbides. ACS Nano 2012;6:1322–31.
[13] Naguib M, Kurtoglu M, Presser V, Lu J, Niu J, Heon M, et al. Two-dimensional nanocrystals produced by exfoliation of Ti3AlC2. Advanced Materials 2011;23:4248–53.
[14] Zha X-H, Yin J, Zhou Y, Huang Q, Luo K, Lang J, et al. Intrinsic structural, electrical, thermal, and mechanical properties of the promising conductor Mo2C MXene. The Journal of Physical Chemistry C 2016;120:15082–8.
[15] Li X, Yin X, Liang S, Li M, Cheng L, Zhang L. 2D carbide MXene Ti2CTX as a novel high-performance electromagnetic interference shielding material. Carbon 2019;146:210–7.
[16] Wang X, Koirala S, Xu L, Li Q, Wang D, Qi X, et al. Advancements in emerging MXene-integrated nanocomposite coatings: Unraveling defect-free microstructure for superior tribological, mechanical, and anti-aging features. Progress in Organic Coatings 2024;188:108206.

[17] Come J, Xie Y, Naguib M, Jesse S, Kalinin SV, Gogotsi Y, et al. Nanoscale elastic changes in 2D Ti3C2Tx (MXene) pseudocapacitive electrodes. Advanced Energy Materials 2016;6:1502290.
[18] Ashton M, Mathew K, Hennig RG, Sinnott SB. Predicted surface composition and thermodynamic stability of MXenes in solution. The Journal of Physical Chemistry C 2016;120:3550–6.
[19] Zhao C, Zhou M, Yu H. Interfacial combination of Ti3C2Tx MXene with waterborne epoxy anticorrosive coating. Applied Surface Science 2022;572:150894.
[20] Krishnan U, Kaur M, Singh K, Kumar M, Kumar A. A synoptic review of MoS2: Synthesis to applications. Superlattices and Microstructures 2019;128:274–97.
[21] Yuan S, Linas S, Journet C, Steyer P, Garnier V, Bonnefont G, et al. Pure & crystallized 2D Boron Nitride sheets synthesized via a novel process coupling both PDCs and SPS methods. Scientific Reports 2016;6:1–9.
[22] Shekhirev M, Shuck CE, Sarycheva A, Gogotsi Y. Characterization of MXenes at every step, from their precursors to single flakes and assembled films. Progress in Materials Science 2021;120:100757.
[23] Verger L, Xu C, Natu V, Cheng H-M, Ren W, Barsoum MW. Overview of the synthesis of MXenes and other ultrathin 2D transition metal carbides and nitrides. Current Opinion in Solid State and Materials Science 2019;23:149–63.
[24] Meshkian R, Näslund L-Å, Halim J, Lu J, Barsoum MW, Rosen J. Synthesis of two-dimensional molybdenum carbide, Mo2C, from the gallium based atomic laminate Mo2Ga2C. Scripta Materialia 2015;108:147–50.
[25] Chen X, Zhao Y, Li L, Wang Y, Wang J, Xiong J, et al. MXene/polymer nanocomposites: preparation, properties, and applications. Polymer Reviews 2021;61:80–115.
[26] Qiang Y, Ran B, Li M, Xu Q, Peng J. GO-functionalized MXene towards superior anti-corrosion coating. Journal of Colloid and Interface Science 2023;642:595–603.
[27] Cao H, Fang M, Jia W, Liu X, Xu Q. Remarkable improvement of corrosion resistance of silane composite coating with Ti3C2Tx MXene on copper. Composites Part B: Engineering 2022;228:109427.
[28] Lou D, Chen H, Liu J, Wang D, Wang C, Jasthi BK, et al. Improved Anticorrosion Properties of Polyurethane Nanocomposites by Ti3C2T x MXene/Functionalized Carbon Nanotubes for Corrosion Protection Coatings. ACS Applied Nano Materials 2023.
[29] Alhabeb M, Maleski K, Anasori B, Lelyukh P, Clark L, Sin S, et al. Guidelines for synthesis and processing of two-dimensional titanium carbide (Ti3C2T x MXene). Chemistry of Materials 2017;29:7633–44.
[30] Mahmood M, Rasheed A, Ayman I, Rasheed T, Munir S, Ajmal S, et al. Synthesis of ultrathin MnO2 nanowire-intercalated 2D-MXenes for high-performance hybrid supercapacitors. Energy & Fuels 2021;35:3469–78.
[31] Wang X, Tang F, Cao Q, Qi X, Pan H, Lin Z, et al. Nano-modified functional composite coatings for metallic structures: Part II—Mechanical and damage tolerance. Surface and Coatings Technology 2020:126274. https://doi.org/10.1016/j.surfcoat.2020.126274.
[32] Smaoui H, Mir LE, Guermazi H, Agnel S, Toureille A. Study of dielectric relaxations in zinc oxide-epoxy resin nanocomposites. Journal of Alloys and Compounds 2009;477:316–21.
[33] Michler GH, Von Schmeling H-HK-B. The physics and micro-mechanics of nano-voids and nano-particles in polymer combinations. Polymer 2013;54:3131–44.
[34] Skaug MJ, Wang L, Ding Y, Schwartz DK. Hindered nanoparticle diffusion and void accessibility in a three-dimensional porous medium. ACS Nano 2015;9:2148–56.
[35] Tanzadeh R, Tanzadeh J, Tahami SA, others. Experimental study on the effect of basalt and glass fibers on behavior of open-graded friction course asphalt modified with nano-silica. Construction and Building Materials 2019;212:467–75.
[36] Fu T, Tang X, Cai Z, Zuo Y, Tang Y, Zhao X. Correlation research of phase angle variation and coating performance by means of Pearson's correlation coefficient. Progress in Organic Coatings 2020;139:105459.
[37] Wang X, Tang F, Qi X, Lin Z. Mechanical, electrochemical, and durability behavior of graphene nano-platelet loaded epoxy-resin composite coatings. Composites Part B: Engineering 2019:107103.
[38] Monetta T, Acquesta A, Bellucci F. Graphene/epoxy coating as multifunctional material for aircraft structures. Aerospace 2015;2:423–34.
[39] Wang X, Pearson M, Pan H, Li M, Zhang Z, Lin Z. Nano-modified functional composite coatings for metallic structures: Part I-Electrochemical and barrier behavior. Surface and Coatings Technology 2020:126286. https://doi.org/10.1016/j.surfcoat.2020.126286.

[40] Wang X, Lin Z. Morphologic and synergistic effects of GNP/NS binary-filler-based multifunctional coatings with robust anti-corrosion and hydrophobic properties. Progress in Organic Coatings 2021;157:106286.
[41] Ammar S, Ramesh K, Ma I, Farah Z, Vengadaesvaran B, Ramesh S, et al. Studies on SiO2-hybrid polymeric nanocomposite coatings with superior corrosion protection and hydrophobicity. Surface and Coatings Technology 2017;324:536–45.
[42] Li Y, Yang Z, Qiu H, Dai Y, Zheng Q, Li J, et al. Self-aligned graphene as anticorrosive barrier in waterborne polyurethane composite coatings. Journal of Materials Chemistry A 2014;2:14139–45.
[43] Wang X, Lin Z. Robust, hydrophobic anti-corrosion coating prepared by PDMS modified epoxy composite with graphite nanoplatelets/nano-silica hybrid nanofillers. Surface and Coatings Technology 2021;421:127440.
[44] Stafford O, Hinderliter B, Croll S. Electrochemical impedance spectroscopy response of water uptake in organic coatings by finite element methods. Electrochimica Acta 2006;52:1339–48.
[45] Gupta A, Kumar N, Sachdeva A. FACTORS AFFECTING THE AGEING OF POLYMER COMPOSITE: A STATE OF ART. Polymer Degradation and Stability 2024:110670.
[46] Plazek D, Frund Jr Z. Epoxy resins (DGEBA): The curing and physical aging process. Journal of Polymer Science Part B: Polymer Physics 1990;28:431–48.
[47] Xia W, Xue H, Wang J, Wang T, Song L, Guo H, et al. Functionlized graphene serving as free radical scavenger and corrosion protection in gamma-irradiated epoxy composites. Carbon 2016;101:315–23.
[48] Kacem I, Daoudi M, Dridi W, Sellemi H, Harzli K, De Izzara G, et al. Effects of neutron–gamma radiation on the free radical contents in epoxy resin: upconversion luminescence and structural stabilization. Applied Physics A 2019;125:1–9.

Figure Captions

Table Captions